Homogenizing microwave illumination in thermoacoustic tomography by a linear-to-circular polarizer based on frequency selective surfaces

Yu He, , Yuecheng Shen, , Xiaohua Feng, , Changjun Liu, and , and Lihong V. Wang

Citation: Appl. Phys. Lett. **111**, 063703 (2017); doi: 10.1063/1.4993942
View online: http://dx.doi.org/10.1063/1.4993942
View Table of Contents: http://aip.scitation.org/toc/apl/111/6
Published by the American Institute of Physics

Homogenizing microwave illumination in thermoacoustic tomography by a linear-to-circular polarizer based on frequency selective surfaces

Yu He,[1,2] Yuecheng Shen,[1] Xiaohua Feng,[1] Changjun Liu,[2,a)] and Lihong V. Wang[1,a)]
[1]*Caltech Optical Imaging Laboratory, Andrew and Peggy Cherng Department of Medical Engineering, Department of Electrical Engineering, California Institute of Technology, Pasadena, California 91125, USA*
[2]*School of Electronics and Information Engineering, Sichuan University, Chengdu 610041, China*

(Received 2 July 2017; accepted 31 July 2017; published online 9 August 2017)

A circularly polarized antenna, providing more homogeneous illumination compared to a linearly polarized antenna, is more suitable for microwave induced thermoacoustic tomography (TAT). The conventional realization of a circular polarization is by using a helical antenna, but it suffers from low efficiency, low power capacity, and limited aperture in TAT systems. Here, we report an implementation of a circularly polarized illumination method in TAT by inserting a single-layer linear-to-circular polarizer based on frequency selective surfaces between a pyramidal horn antenna and an imaging object. The performance of the proposed method was validated by both simulations and experimental imaging of a breast tumor phantom. The results showed that a circular polarization was achieved, and the resultant thermoacoustic signal-to-noise was twice greater than that in the helical antenna case. The proposed method is more desirable in a waveguide-based TAT system than the conventional method. *Published by AIP Publishing.* [http://dx.doi.org/10.1063/1.4993942]

Microwave induced thermoacoustic tomography (TAT) is a non-ionizing imaging modality with potential to detect breast tumors.[1–9] It relies on the detection of ultrasonic waves, generated by thermal expansion of tissue constituents that absorb sub-microsecond pulses of electromagnetic radiation at a microwave frequency. Tumors with higher dielectric loss absorb more energy and generate stronger thermoacoustic waves than the surrounding healthy tissues do, which provides a high microwave contrast.[10] The purpose of TAT is to reconstruct the distribution of the microwave absorption and locate the positions of the tumors in breasts from a set of measured acoustic signals. In practice, the microwave at 3 GHz is often adopted since its $1/e$ penetration depths for fat (low water content) and muscle (high water content) are 9.0 and 1.2 cm,[11] respectively, which is suitable for breast tumor detection.

In order to achieve a sufficient microwave energy output for TAT, a high-peak-power pulsed microwave magnetron equipped with a rectangular waveguide output port is usually used.[12–15] Then, a pyramidal horn antenna with a rectangular waveguide input port is used as the transmitting antenna to illuminate an object. However, a pyramidal horn antenna, which radiates linearly polarized waves, causes image distortion in the reconstructed images due to inhomogeneous illumination.[14,16–18] A helical antenna, radiating circularly polarized waves, has been proved to provide more homogenous illumination.[18] The reconstructed images, as a direct reflection of the microwave energy absorption in the object, present better quality under circularly polarized illumination than those under linearly polarized illumination.[18] However, when a coaxial-fed helical antenna is applied to a waveguide-based TAT system, it requires a coaxial-to-waveguide adapter and a coaxial connector to couple the microwave energy from the magnetron. Both the adapter and the connector are power-limiting components, which may cause sparks and cannot transfer the entire power from the magnetron to the helical antenna. Moreover, they produce non-negligible insertion loss when conducting microwaves. The efficiency of a helical antenna is also much lower than that of a horn antenna due to its structure.[19] All these significant energy-coupling losses lead to inefficient thermoacoustic signal generation. Even worse is that the adapter and the connector may break down when exposed to high-power microwaves. Thus, a safe and efficient method that generates circularly polarized waves without any coaxial-based and coaxial-fed microwave components is desired to improve the performance of antenna illumination in TAT.

Recently, frequency selective surfaces (FSSs) have been introduced for polarization applications in the microwave regime.[20–25] The unit-cell geometries of FSS include crosses,[21,22] meander lines,[23] and split rings.[24,25] In addition to providing the linear-to-circular polarization transformation, an FSS polarizer has the advantages of low profile, ease of fabrication, stable performance for different incident angles, and relatively low energy loss, making it well suited for TAT.

In this letter, we report an implementation of circularly polarized illumination in TAT by inserting a single-layer FSS polarizer between the pyramidal horn antenna and the imaging object. The principle of operation is shown in Fig. 1. The generated wave from the horn antenna is linearly polarized at 45° to the x-axis and can be decomposed into two orthogonal components E_x^{in} and E_y^{in}. The unit cell of the proposed FSS consists of a Jerusalem-cross. The arms of the cross in the unit cell have different lengths along the orthogonal directions so that the transmitted wave components with orthogonal polarizations (E_x^{in} and E_y^{in}) experience different refractive indexes, resulting in a phase difference. If E_x^{out} and E_y^{out} are equal in magnitude and have a phase difference of 90°, a

a)Authors to whom correspondence should be addressed: cjliu@scu.edu.cn and LVW@caltech.edu

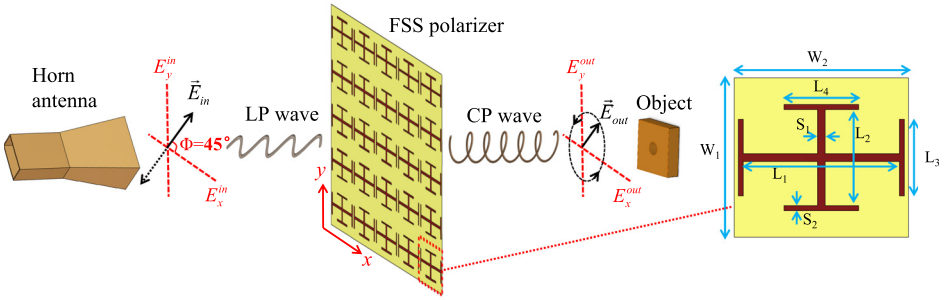

FIG. 1. Principle of operation. The FSS polarizer, acting as a quarter-wave plate, transforms a linearly polarized (LP) wave radiating from a slant pyramidal horn antenna into a circularly polarized (CP) wave. Parameters of the unit cell: $S_1 = 1.5$, $S_2 = 1.0$, $W_1 = 31.1$, $W_2 = 35$, $L_1 = 31.3$, $L_2 = 18.9$, $L_3 = 15$, and $L_4 = 15$ (Unit: mm).

circularly polarized wave is generated before illuminating the imaging object.

The proposed FSS polarizer was printed on a microwave substrate (Rogers 5880) with a permittivity of 2.2, a loss tangent of 0.0009, and a thickness of 0.786 mm. The full-wave numerical simulation of the FSS polarizer was performed using CST Microwave Studio. Since the FSS polarizer has a periodical structure, in order to reduce the computational time, we simulated only one unit cell with periodic boundary conditions in the polarizer design. The operating frequency of the magnetron (S-Band, MG5240) used in the TAT system is 3050 MHz ± 25 MHz, and therefore, the FSS polarizer should be designed to work between 3025 MHz and 3075 MHz. By tuning the dimensions of the cross and the unit cell, the optimal parameters of the unit cell are obtained and depicted in the caption of Fig. 1. The transmission magnitudes and phases of E_x^{out} and E_y^{out} are shown in Fig. 2(a). At 3050 MHz, the magnitudes of both the orthogonal electric field components are the same with an insertion loss of around 3 dB and the phase difference between the two components is around 90°, which meets the requirements to convert a linear polarization into a circular polarization. Generally, a perfect circular polarization can only be achieved at a single frequency. Thus, the axial ratio (AR) ≤ 3 dB bandwidth was used to define the circular polarization bandwidth, where the AR was calculated as the ratio of the major axis to the minor axis.[23] Considering that the incident field may not be tilted at exactly 45° due to the installation inaccuracy in practice, we also studied the robustness of the polarizer under normal but deflected incident angles deviating from 45°, and the results are shown in Fig. 2(b). According to the working frequency of the magnetron, the required AR ≤ 3 dB band is from 3025 MHz to 3075 MHz. The AR ≤ 3 dB bandwidths indicate that the polarizer is robust at illuminating angles varying from 40° to 50°.

Having designed the FSS polarizer, we combined the polarizer with a pyramidal horn antenna and quantified the performance by imaging a breast tumor phantom. The tumor phantom used in the simulation is shown in Fig. 3(a). The dielectrically homogeneous cylinder with a relative permittivity of 70 and a conductivity of 2.0 S/m mimicked a breast tumor. The diameter of the cylinder was 8 mm, and the length was 10 mm. The surrounding cube with a relative permittivity of 5 and a conductivity of 0.1 S/m mimicked adipose tissue. The tumor was placed off-centered and embedded in the adipose tissue. First, a pyramidal horn antenna (WR-284) with an opening size of 108 mm × 72 mm was used to illuminate the phantom in the z direction. The polarization of the horn antenna was in the y direction. The simulated microwave absorption of the phantom is shown in Fig. 3(b). The tumor is not homogenously irradiated, and the microwave absorption is much stronger at the two ends along the y axis and weaker in between, which exhibits a "bipolar" pattern. Then, the proposed FSS polarizer was inserted between the pyramidal horn antenna and the phantom. In order to cover the aperture of the pyramidal horn antenna, the FSS polarizer was composed of

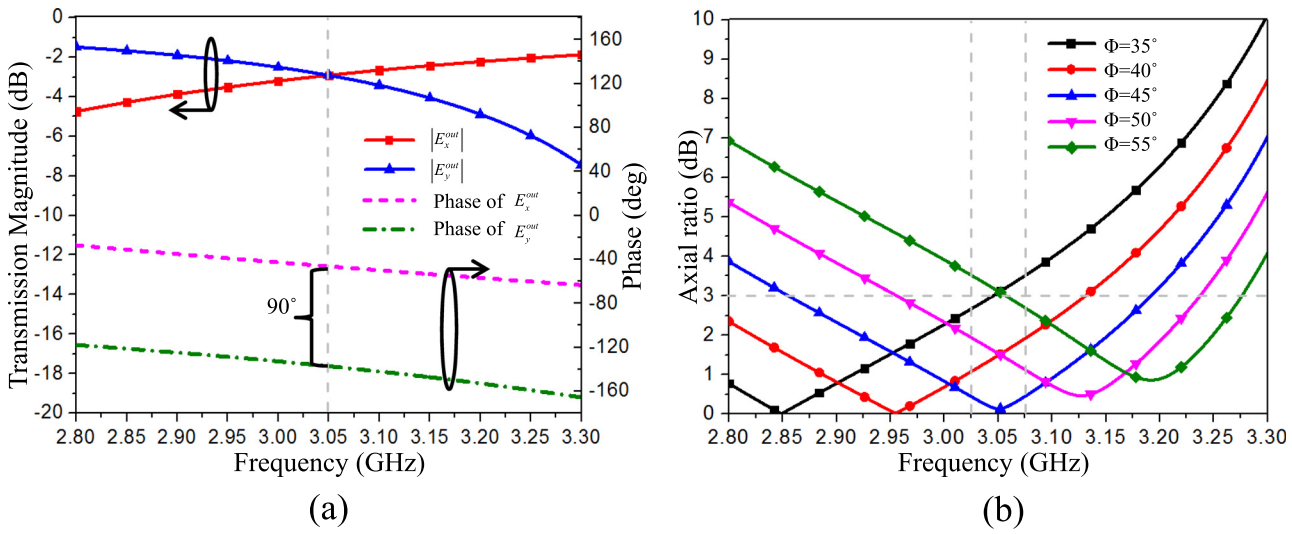

FIG. 2. (a) Transmission magnitude and phase of the orthogonal components of the E-field. The magnitudes of both electric fields are the same, and the phase difference is 90° at 3.05 GHz. (b) Axial ratios of the proposed polarizer under a normal but deflected incident LP wave.

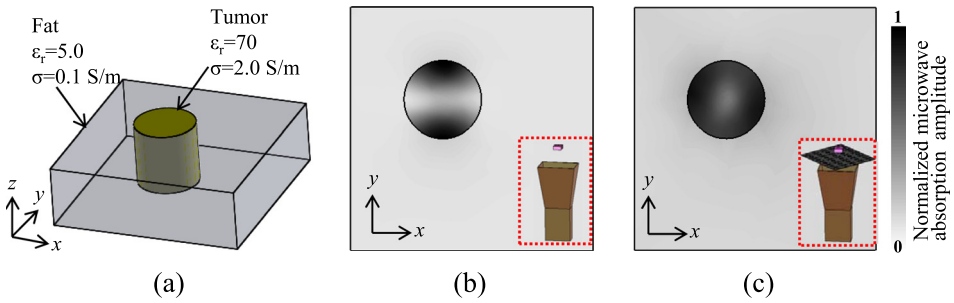

FIG. 3. (a) Simulated tumor phantom model. The cylinder placed off-centered mimics a breast tumor, and the surrounding fat mimics normal breast tissue. Simulated microwave absorption of the tumor phantom irradiated by a horn antenna (b) without and (c) with an FSS polarizer.

5 × 5 unit cells, making the total size of the polarizer equal to 175 mm × 156 mm. The FSS polarizer was placed on top of the antenna and has a 45° angle with respect to the *y* direction. Considering that the delivered energy to the phantom decreases inversely with respect to the distance between the antenna and the phantom, the phantom requires to be placed as close to the aperture of the horn antenna as possible. Taking the practical experimental condition into consideration, the FSS polarizer was placed 3 cm away on top of the antenna and the phantom was placed 2 cm above the polarizer. Figure 3(c) shows the simulated microwave absorption of the phantom. The tumor is more homogenously illuminated since the linearly polarized wave emitting from the horn antenna is transformed into a circularly polarized wave by the FFS polarizer. The "bipolar" pattern no longer exists here, and a nearly homogenous pattern is observed. We note that there exists a slight asymmetry for the microwave absorption along the two orthogonal directions, i.e., *x* and *y* directions. This is because when we designed a unit cell of the FSS polarizer, we used a plane wave to excite the periodical structure for ease of simulation. However, when the FSS polarizer was applied to the pyramidal horn antenna, it was placed in the near field of the antenna and the wave reaching the polarizer could not be regarded as a plane wave. As a result, the wave at the position of the phantom was not perfectly circularly polarized. Nevertheless, the simulated results show that applying the FSS polarizer to the horn antenna improves the homogeneity of the microwave illumination.

The setup for experimental validation is shown in Fig. 4(a). Pulsed microwaves with a peak power of 60 kW generated from the magnetron were coupled into the waveguide. The microwave pulse width was 0.5 μs, and the pulse repetition rate was 10 Hz. A waveguide circulator with three ports and a microwave load was used to protect the magnetron. The incident microwaves from port 1 were only transmitted to port 2. The microwaves reflected from port 2 were transmitted to port 3, where a matched microwave load was connected and absorbed most of the reflected energy. Thus, no reflected energy went back to the magnetron. The microwave radiating parts connected to port 2 had three cases here: (1) a pyramidal horn antenna; (2) a helical antenna connected through a coaxial-to-waveguide adapter and an N-type connector; (3) a pyramidal horn antenna with an FSS polarizer on top of it. The breast tumor phantom in the experiment was made of porcine fat and had an off-centered hole filled with a water-based gel. As with the simulation, the cylinder gel, made of 3% agar powder and 97% water, mimicked a breast tumor and the porcine fat mimicked normal breast tissue. The diameter of the cylinder was 8 mm. Mineral oil, which has very low absorption to microwaves, was used as

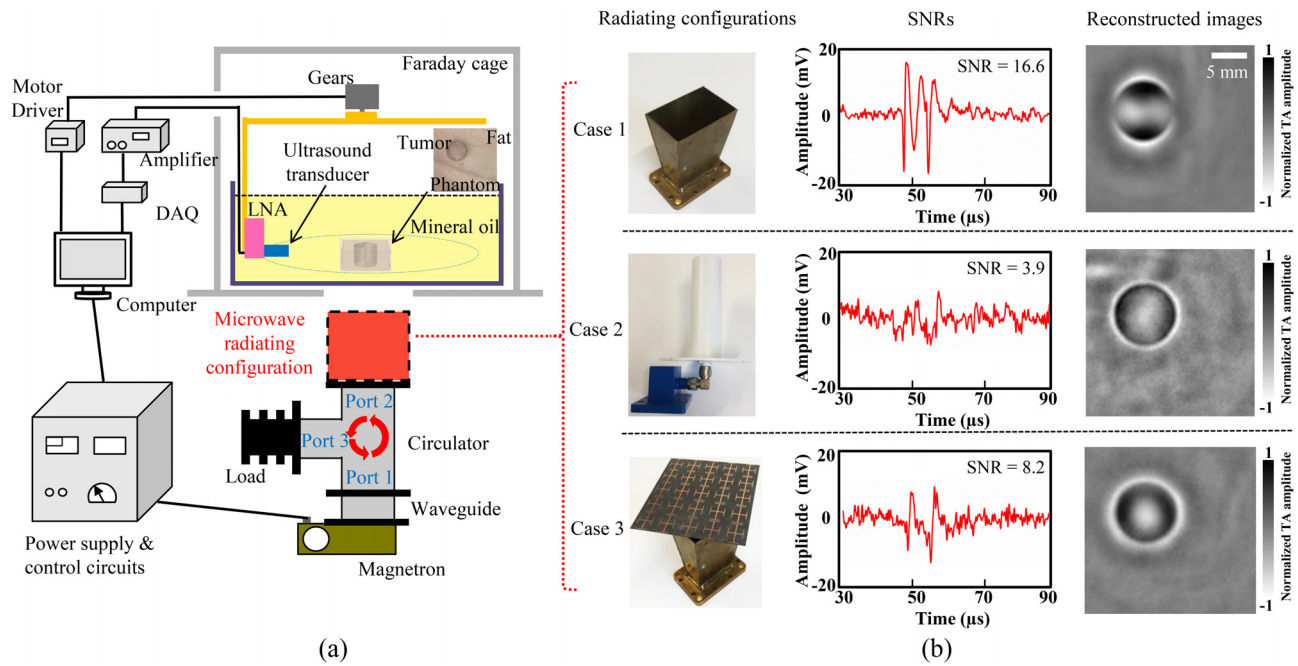

FIG. 4. (a) Experimental setup. (b) The three different radiating configurations, the corresponding SNRs, and the reconstructed images.

the acoustic coupling medium. An ultrasonic transducer with a center frequency of 2.25 MHz and a diameter of 6 mm (V323, Panametrics-NDT) was used to detect the induced thermoacoustic signals. The transducer, fixed on a rotational apparatus and controlled by a motor, performed a circular scan of the phantom with a step size of 1.8°. The generated thermoacoustic signals received by the transducer were first transferred to a self-made low noise amplifier (LNA) with a gain of 20 dB, then amplified by a second 50 dB amplifier (5072 PR, Panametrics), directed to a data-acquisition card (DAQ) with a sampling frequency of 20 MHz, averaged 10 times at each scanning stop, and finally transferred to a computer for image reconstruction. Transducer scanning, pulse triggering, and data acquisition were all synchronized by a LabVIEW program.

We conducted several phantom experiments by using the three different radiating configurations. The SNR was obtained after 10 times averaging, and the cross-sectional thermoacoustic images of the phantom were reconstructed using the back-projection algorithm.[26] The measured results are shown in Fig. 4(b). For case 1, where the pyramidal horn antenna is applied, the SNR is as high as 16.6. However, the linearly polarized illumination causes the tumor phantom to split vertically into two parts, and the horizontal boundary of the tumor is indiscernible in the reconstructed image. The image distortion caused by the inhomogeneous microwave field provided by the pyramidal horn antenna can be suppressed by using a circularly polarized antenna, as shown in case 2, where a helical antenna is applied. The tumor phantom is more homogeneously illuminated, and the "split" pattern in the reconstructed image for case 1 no longer exists here. However, due to the losses of the helical antenna, the coaxial-to-waveguide adapter, and the N-type connector, the SNR drops dramatically to 3.9, which makes the reconstructed image for case 2 quite noisy. For case 3, the proposed FSS polarizer was placed on top of the pyramidal horn antenna and slanted at 45°. The distances among the horn antenna, the polarizer, and the phantom were in accordance with those of the simulation. Since the tumor phantom was also illuminated by waves with a circular polarization, the "split" pattern disappears, and the boundaries of the reconstructed images are clearer for the whole circumference of the tumor phantom. The reconstructed image matches well with the simulated microwave absorption shown in Fig. 3(c). The SNR for case 3 is 8.2, which is about twice greater than that for case 2.

In order to illuminate the phantom upward, the helical antenna should be designed to operate in the axial mode. Thus, the circumference of a turn on the helical antenna is usually about one wavelength (here, 100 mm at 3 GHz), which indicates that the diameter of the helical antenna is only about 32 mm at 3 GHz. The helical antenna provides a relatively small field of view. Besides providing a circularly polarized illumination, we note that the pyramidal horn antenna (108 mm × 72 mm) loading with the polarizer can provide a larger field of view, which covers a breast better than the helical antenna ($\pi \times 16^2$ mm) does.

Additional challenges lie ahead in regard to reducing the insertion loss of the FSS polarizer. For the current design, about half of the energy was reflected by the proposed FSS polarizer. Implementation of a polarizer by using a multilayered structure is one way to reduce the loss.[22,25] However, the air gaps among the different layers will increase the distance between the phantom and the antenna aperture, which reduces the delivered energy to the phantom significantly. Therefore, designing a single-layer polarizer with lower loss will be a promising direction for TAT applications.

In summary, we implemented circularly polarized illumination in TAT by inserting a single-layer linear-to-circular polarizer based on FSS between the pyramidal horn antenna and the imaging object. Compared to a helical antenna, the proposed microwave transmitting method is more suitable for a waveguide-based TAT system. We anticipate that this method will contribute to clinical breast tumor diagnosis.

This work was supported in part by the China 973 program 2013CB328902 and the China Scholarship Council.

[1]L. V. Wang, X. Zhao, H. Sun, and G. Ku, Rev. Sci. Instrum. **70**(9), 3744 (1999).
[2]R. A. Kruger, K. D. Miller, H. E. Reynolds, W. L. Kiser, Jr., D. R. Reinecke, and G. A. Kruger, Radiology **216**(1), 279 (2000).
[3]F. Gao, Y. Zheng, X. Feng, and C.-D. Ohl, Appl. Phys. Lett. **102**(6), 063702 (2013).
[4]X. Zhu, Z. Zhao, J. Wang, J. Song, and Q. H. Liu, IEEE Trans. Biomed. Eng. **60**(5), 321 (2013).
[5]X. Wang, T. Qin, R. S. Witte, and H. Xin, IEEE Trans. Microwave Theory Techn. **63**(5), 1489 (2015).
[6]X. Feng, F. Gao, and Y. Zheng, Appl. Phys. Lett. **103**(8), 083704 (2013).
[7]F. Ye, Z. Ji, W. Ding, C. Lou, S. Yang, and D. Xing, IEEE Trans. Med. Imag. **35**(3), 839 (2016).
[8]Y. He, Y. Shen, C. Liu, and L. V. Wang, Appl. Phys. Lett. **110**(5), 053701 (2017).
[9]W. Ding, Z. Ji, and D. Xing, Appl. Phys. Lett. **110**(18), 183701 (2017).
[10]M. Lazebnik, L. McCartney, D. Popovic, C. B. Watkins, M. J. Lindstrom, J. Harter, S. Sewall, A. Magliocco, J. H. Booske, and M. Okoniewski, Phys. Med. Biol. **52**(10), 2637 (2007).
[11]M. Xu and L. V. Wang, Med. Phys. **29**(8), 1661 (2002).
[12]A. Mashal, J. H. Booske, and S. C. Hagness, Phys. Med. Biol. **54**(3), 641 (2009).
[13]H. Ke, T. N. Erpelding, L. Jankovic, C. Liu, and L. V. Wang, J. Biomed. Opt. **17**(5), 056010 (2012).
[14]L. Huang, L. Yao, L. Liu, J. Rong, and H. Jiang, Appl. Phys. Lett. **101**(24), 244106 (2012).
[15]J. Song, Z. Zhao, J. Wang, X. Zhu, J. Wu, Z.-P. Nie, and Q. H. Liu, Prog. Electromagn. Res. **140**, 385 (2013).
[16]M. Pramanik, G. Ku, C. Li, and L. V. Wang, Med. Phys. **35**(6), 2218 (2008).
[17]C. Li, M. Pramanik, G. Ku, and L. V. Wang, Phys. Rev. E **77**(3), 031923 (2008).
[18]Y. He, C. Liu, L. Lin, and L. Wang, IEEE Antennas Wireless Propag. Lett. **16**, 1593–1596 (2017).
[19]H. A. Wheeler, Proc. IRE **35**(12), 1484 (1947).
[20]K. Karkkainen and M. Stuchly, IEE Proc.-Microwaves Antennas Propag. **149**(56), 248 (2002).
[21]G. I. Kiani and V. Dyadyuk, presented at the *2010 European Microwave Conference, September 28–30* (EUMC, Paris, France 2010).
[22]G. Kiani and V. Dyadyuk, presented at the *2012 IEEE Antennas and Propagation Society International Symposium July 8–14* (APSURSI, Chicago, IL, 2012).
[23]P. Fei, Z. Shen, X. Wen, and F. Nian, IEEE Trans. Antennas Propag. **63**(10), 4609 (2015).
[24]M. Euler, V. Fusco, R. Cahill, and R. Dickie, IEEE Trans. Antennas Propag. **58**(7), 2457 (2010).
[25]L. Martinez-Lopez, J. Rodriguez-Cuevas, J. I. Martinez-Lopez, and A. E. Martynyuk, IEEE Antennas Wireless Propag. Lett. **13**, 153 (2014).
[26]M. Xu and L. V. Wang, Phys. Rev. E **71**(1), 016706 (2005).